Chapter 5

Characterization of transparent micro-objects

4.1 Introduction

So far the use of digital holography in the characterization of wavefronts for testing of lenses and its use in imaging of refractive index distributions has been discussed. But since digital holography is a technique that provides whole field reconstructions, it can be used as a method foe phase contrast imaging of otherwise transparent objects. Microscopy is the technique of using lenses to view magnified images of samples or objects which cannot be seen with the unaided eye. A basic microscope involves a single lens system that uses only one lens for magnification, and is the original light microscope. It consists of a small, single converging lens. The magnification of the object by a single lens depends upon on its position. Fig. 5.1 shows the different imaging geometries using a single converging lens.

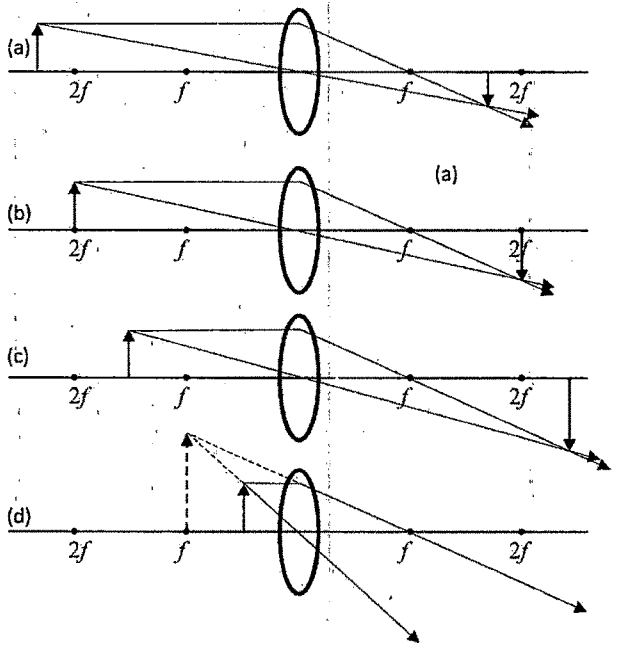

Fig. 5.1: Imaging setup using a single lens

Fig. 5.1(a) shows the object placed at a distance greater than $2f$ from the lens principle plane. This configuration results in an inverted, real and de-magnified image between f and $2f$ on the right hand side of the principle plane. Since the image is real, it can be projected on to screen or captured using a photo-sensitive medium. Fig. 5.1(b) represents the case in which the object is placed between exactly at $2f$ from the lens principle plane. Here unit magnification, real, inverted image will be formed exactly at a distance $2f$ on the RHS of the principle plane. Third case (Fig. 5.1(c)) represents the geometry where real, inverted and magnified image results. The geometry given by Fig. 5.1(d) also results in magnified image. But here the image is erect and virtual. This means that the image is formed on the same side as that of the object. To see this image, another lens, like human eye, has to be used.

Evolution of microscope led to development of multi-lens setup or compound microscope. Most of the compound microscopes use a two-lens system as shown in Fig. 5.2 [5.1].

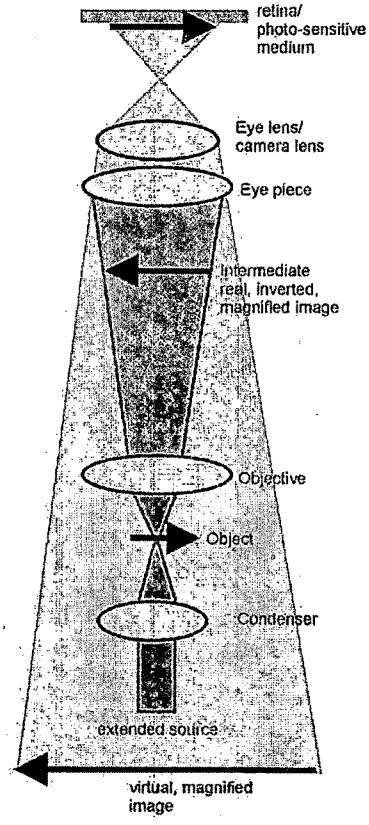

Fig. 5.2: Compound microscope

The compound microscope has two systems of lenses for greater magnification, 1) the ocular or eyepiece lens that one looks into and 2) the objective lens, or the lens closest to the object. Objective lens forms an enlarged real image of the object and the eye piece magnifies the image formed by the objective lens. This results in a virtual image. The total magnification is then the product of the magnifications of both lens systems. The objective lens is a small, round piece of glass which collects the light from a small area of the specimen at a short focal length and directs the light into the tube. The image is then magnified by the ocular lens, which is put up to the eye. Because the objective lens is convex, it focuses and directs light into its center. By contrast, the concave shape of the eye lens serves to spread out the light as it meets the eye, thereby making the image bigger. The condenser is a lens, often implanted into the stage or located just below it, that condenses the light rays from the light source onto the spot that is being examined on the specimen.

The resulting image in both single lens system and two-lens system can be detected directly by the eye, imaged on photographic plates or captured digitally. The most recent development is the digital microscope which uses a CCD camera to focus on the exhibit of interest. The image is shown on a computer screen since the camera is attached to it.

Imaging of living cells is one of the important tasks for which microscopy is used. Live cells generally lack sufficient contrast to be studied successfully; internal structures of the cell are colourless and transparent. So imaging of transparent micro-objects like living cells is an interesting and challenging problem in microscopy. Most of the biological micro-objects are transparent to the visible radiations and do not produce appreciable change to the amplitude of the electromagnetic radiation passing through them. So it becomes difficult to image them with conventional microscopy. The use of chemicals for staining becomes necessary to image them. Another problem with conventional microscopy is that it provides the object information at a particular plane only due to the finite depth of focus of especially larger numerical aperture, high magnification objectives used.

Phase objects like living cells introduces a change to the phase of the electromagnetic radiation depending upon the refractive index as well as the thickness of the specimen. If these phase changes occurring to the probe wavefront can somehow be imaged, this will lead to imaging of the object under investigation. Methods for

imaging phase objects by measuring the phase change occurring to the probe beam are called phase contrast techniques. There are several methods in optical microscopy used for imaging unstained specimens by converting the phase information to amplitude change and most common among them are Zernike and Nomarski methods [5.2-5.4]. Interference techniques can also be used for phase contrast imaging, yielding the quantitative phase values rather than just images. The main disadvantage of interferomertic techniques is the use of phase stepping to yield the quantitative phase information, making them difficult to implement. Digital holography is a tool providing the three dimensional aspects of an object [5.5]. Digital holography utilizes optical recording of holograms on light sensitive semiconductor arrays and their numerical reconstruction by simulating diffraction in a computer [5.6, 5.7]. The numerical reconstruction of holograms directly yields the complex amplitude of the object wavefront and hence the spatial phase distribution [5.5]. It has the added advantage of numerical focusing since each plane in the object has contributed to the hologram. Together these properties make Digital Holographic Microscopy (DHM) an attractive tool for imaging transparent micro-objects [5.8-5.18]. DHM is a technique that allows obtaining, from a single recorded hologram, quantitative phase image of living cell with interferometric accuracy. Specifically the optical phase shift induced by the specimen on the transmitted wave front can be regarded as a powerful endogenous contrast agent, depending on both the thickness and the refractive index of the sample. Here the use of DHM with angular spectrum propagation reconstruction for imaging transparent micro-objects is described [5.18].

5.2 Digital Holographic Microscope

Fig. 5.3 shows the experimental setup employed to implement DHM using low power laser sources. A random linearly polarized He-Ne laser source providing CW output at 611nm and maximum output power of 2mW is utilized in the experiments.

The output from the laser source is expanded using a spatial filtering assembly and collimated. This is then split into two using a non-polarizing beamsplitter. One of the beams acts as the reference beam and the other beam is condensed and passed through the object under investigation. In the course of this work transparent and semi transparent objects were used. A microscopic objective magnifies the object. A CCD camera was placed in the path of the object beam. The object beam and the reference

beam are made to interfere at the CCD camera using a Mach-Zehnder configuration. A similar kind of focusing lens and microscopic objective is introduced in the object beam path to match the curvatures of the beams. A slight angle is introduced between the object and reference beams to achieve off-axis geometry. The DHM co-ordinate system is shown in Fig. 5.4.

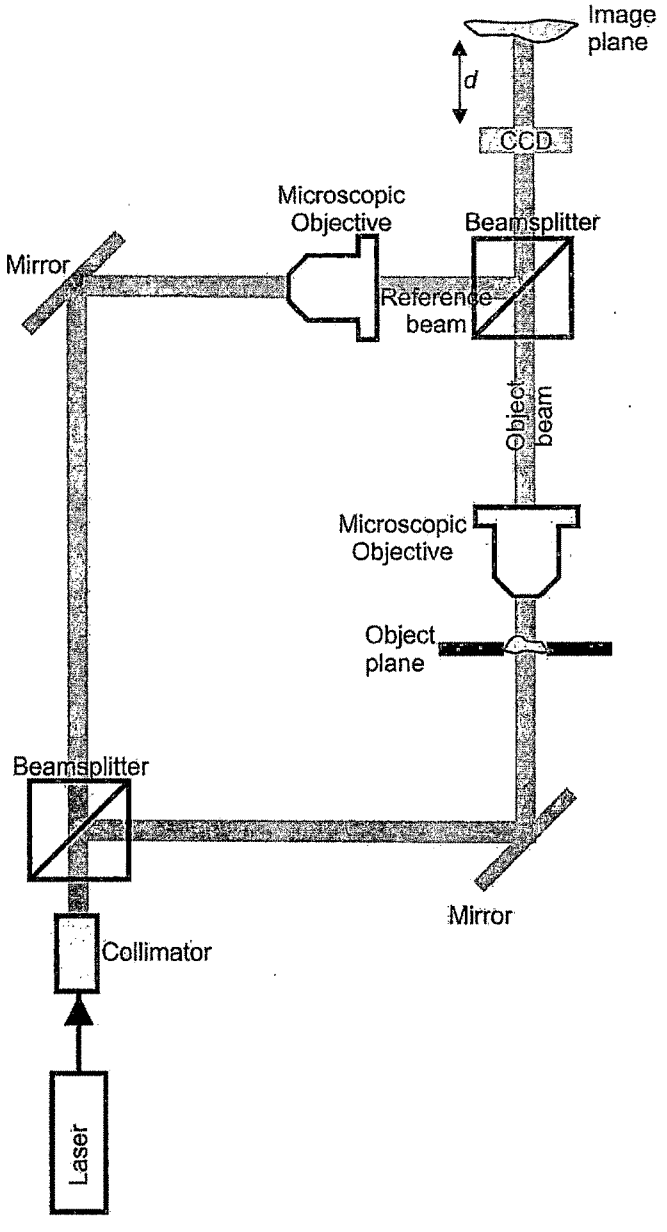

Fig. 5.3: Experimental setup for Digital interference Holographic Microscope

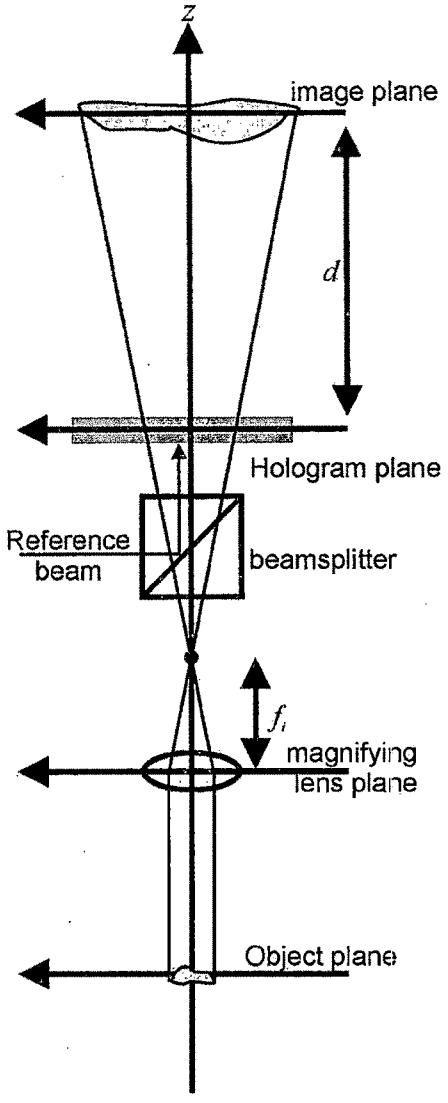

Fig. 5.4: Hologram formation in DHM and co-ordinate system

It can be seen that that the wavefront from the magnified image interferes with the reference wavefront at the detector and the distance between the image plane and hologram plane is *d*. The recording device could be kept anywhere along the interference field distribution, since digital holography has the advantage of numerical focusing.

5.3 Reconstruction of digital holograms

Her e since the distance between the object plane and the hologram plane is small as well as since the fringe system is very pronounced, angular spectrum propagation approach to scalar diffraction theory described in section 2.7.5 is used for numerical reconstruction of holograms.

5.4 Computation of intensity and phase

As mentioned in Chaper 2, numerical reconstruction of digital holograms yields the complex amplitude of the object wavefront. Once the complex amplitude is available, the state or phase of the wavefront as well its intensity could be computed as shown in Section 2.8. For DHM to obtain phase contrast images, the phases with and without the object present are computed and the phase difference is calculated using

$$\begin{aligned} \Delta\phi(x,y) &= \phi_i(x,y) - \phi_f(x,y) \qquad \text{if } \phi_i > \phi_f \\ &= \phi_i(x,y) - \phi_f(x,y) + 2\pi \quad \text{if } \phi_f > \phi_i \end{aligned} \tag{79}$$

where ϕ_i is the phase of the object in the first state and the ϕ_f is phase for the second state. The phase takes values between $-\pi$ and π. So the computed phase difference has to be unwrapped if the phase change is more than 2π.

5.5 Computation of optical path length (OPL) change

This phase difference acquired by a ray propagating in the z direction (Fig. 2) given in Eq. (79) is proportional to the optical path length change according to

$$\Delta\phi(x,y) = \frac{2\pi}{\lambda}\Delta n(x,y)\Delta L(x,y) \tag{80}$$

where $\Delta n(x, y)$ is the refractive index change and $\Delta L(x, y)$ is the thickness change. The change in optical path length or OPL ($\Delta n(x, y) \times \Delta L(x, y)$) is brought about by a change in physical thickness or by a change in refractive index of the object under study. If any one of these quantities is known the other can be determined. For an object undergoing a change in refractive index, while keeping its physical thickness a constant, Eq. (80) can be used to determine change in refractive index distribution occurring between the exposures.

5.6 Experimental investigations

Experiments were conducted on static and dynamic systems. First of the systems studied was static systems. First of the investigated systems was two plastic plates stuck together, with air bubbles in between. This is a completely static system. The second of the systems investigated was onion skin cells, whose dynamics are very slow. Third of the investigated systems was the fast dynamics of a non-biological object. The object investigated was a letter embossed on section of Acrylic sheet.

5.6.1 Investigations on static object

First of the static object tested was the laser print out taken on a transparency sheet without the magnification lens It was kept in the object arm of the digital holographic microscope shown in Fig. 5.4. Holograms of the object were recorded. The CCD camera used had 570×760 square pixels of 6.25μ pixel pitch and 8-bit dynamic range. The wavelength of the source was 611nm. The object was kept 120mm from the hologram. Fig. 5.5a shows the reconstructed intensity distribution at the object plane clearly showing the letters. Fig. 5.5b shows the phase distribution at the object plane for this object.

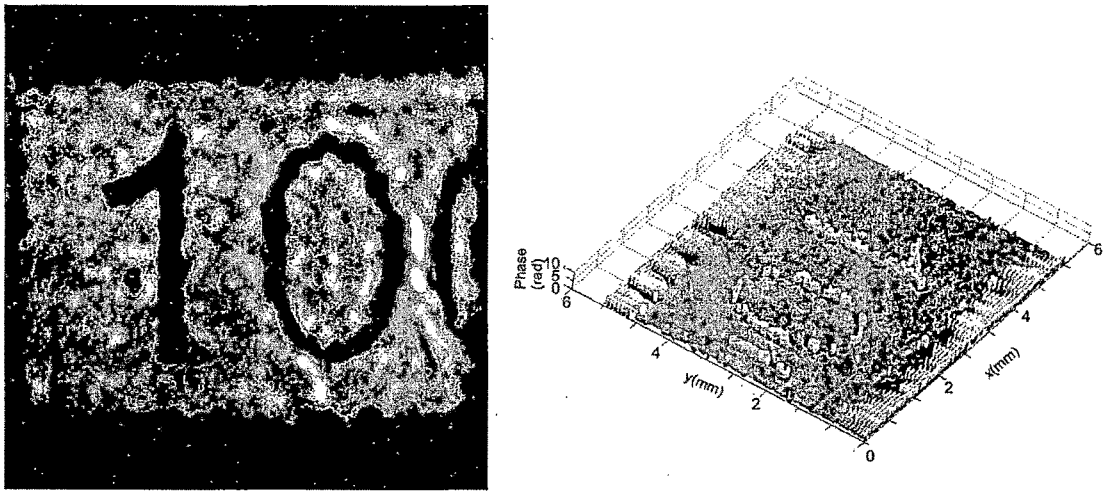

(a) (b)

Fig. 5.5: Reconstructed (a) intensity and (b) phase distribution for laser print on a transparency. Object was kept 120mm from the CCD plane.

These results clearly show that the method is quite useful in imaging transparent objects, from their phase distributions.

The lateral size of the object can be directly obtained from the lateral extent of the phase distribution. It can be written as

$$\Lambda_L = \frac{N \times \Delta x}{M_L} \tag{81}$$

Where N is the number of pixels the phase distribution extends, Δx is the CCD pixel size and M_L is the lateral magnification of the imaging system. In the case shown in Fig. 5.5 lateral magnification was unity since no magnifying lens was used. The lateral dimensions of the object is determined from the edge detected the phase image. A MATLAB code for edge detection and determination of lateral size was also developed.

The second static object tested was two plastic sheets stuck together, with air bubbles in between. An achromat with 5cm focal length and 25.4mm clear aperture was used for magnification. The objet was kept 7.5cm from the lens so as to achieve a magnification of 2. The CCD plane was 120mm from the object plane. The intensity and phase distribution t the image plane (here the image plane lies 30mm to the right of the CCD plane).

It can be seen from Fig. 5.6 that the phase image provides a better picture of the object. The edge detection of the phase images was done after unwrapping. Fig. 5.7 shows the edge detected image of Fig. 5.6b. Edge detection was performed using Sobel method. Measured lateral dimensions using Eq. (5.3) for some of the objects is also shown.

The optical path length distribution provides information on the axial extent of the object under investigation. This information is obtained from the unwrapped phase map of the object phase distribution. Fig. 5.8 shows the axial extent if the object in Fig. 5.6a

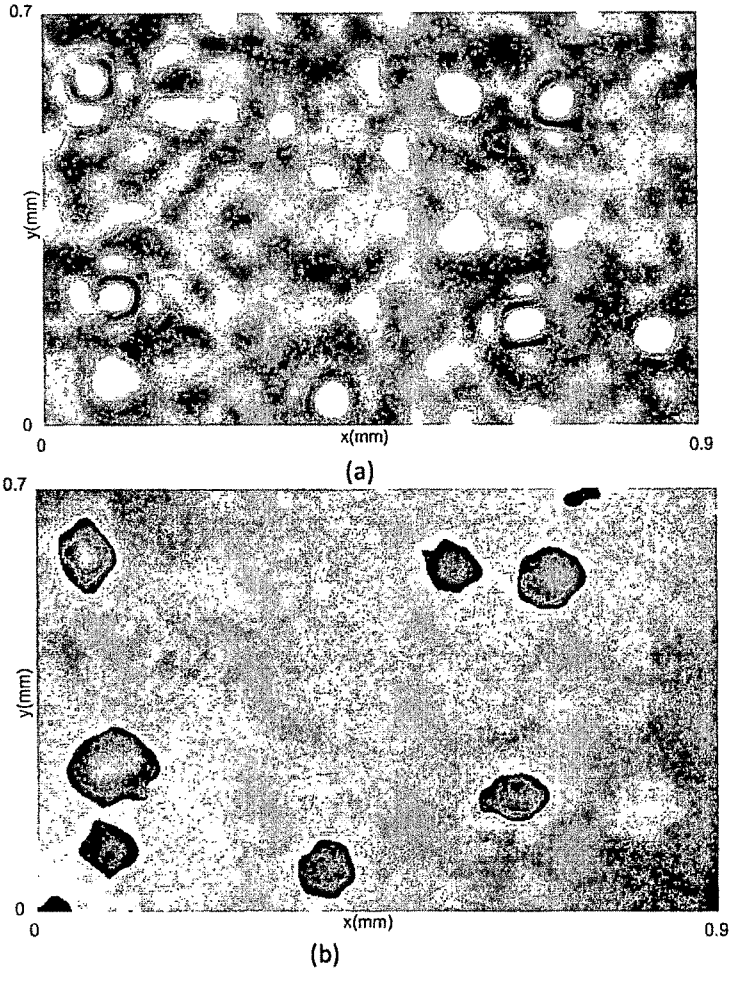

Fig. 5.6: Reconstructed (a) intensity and (b) phase at the image plane for two plastic sheets stuck together with air bubbles in between.

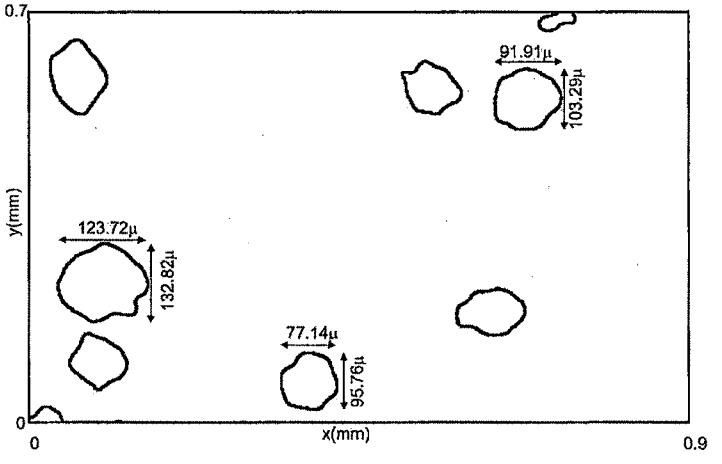

Fig. 5.7: Edge detected image obtained from the unwrapped phase map of the phase distribution shown in Fig. 5.6b.

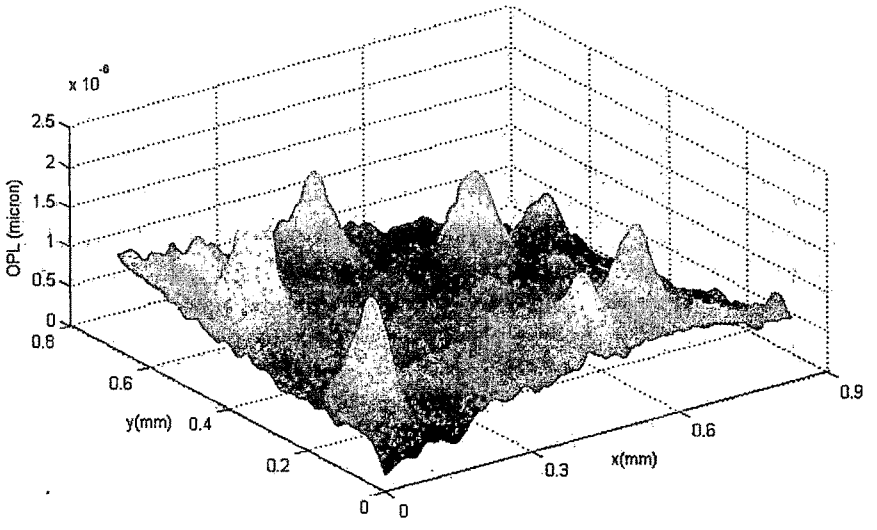

Fig. 5.8: Optical path length distribution of the object in Fig. 5.6a

5.6.2 Investigations on onion cells

Onion skin cells vary in size from 250 to 400 microns and mostly rectangular in shape (Fig. 5.9) and thickness of several microns.

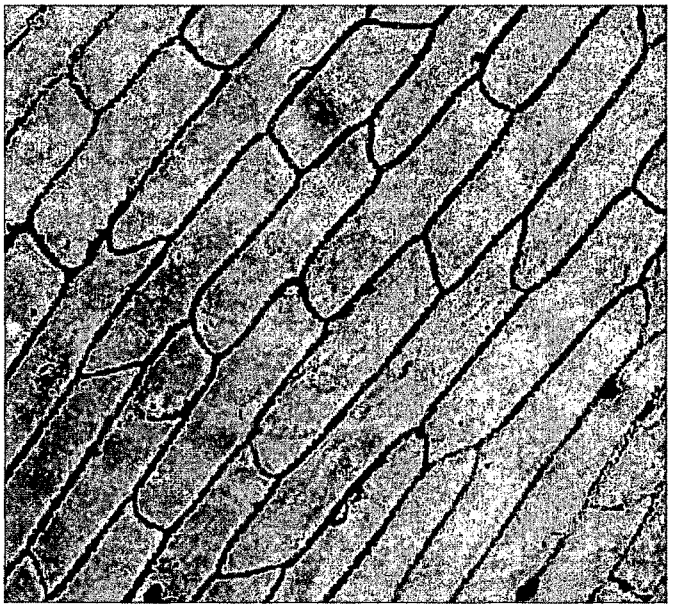

Fig. 5.9: Onion skin cells under bright field microscope

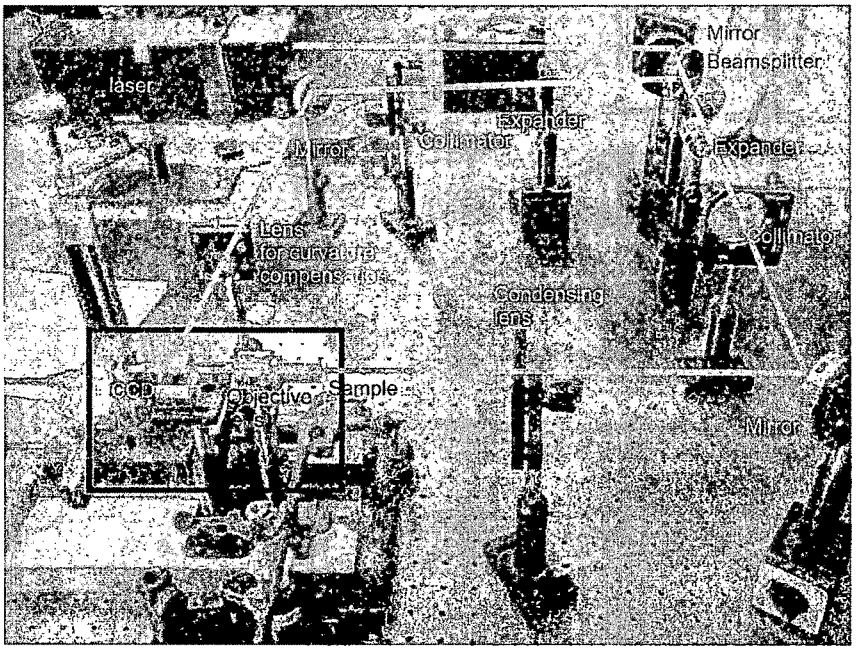

(a)

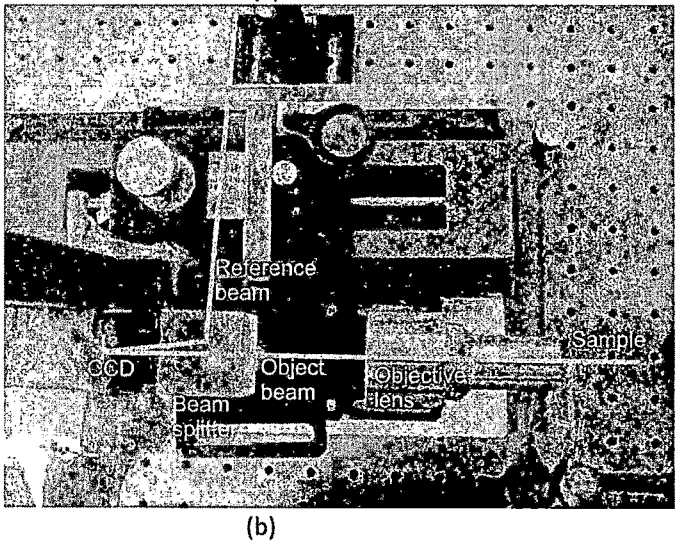

(b)

Fig. 5.10: (a) Photograph of the experimental setup of DHM to image micro-object (b) Close-up view of the portion marked in the rectangle in Fig. 5.9a.

Experimental setup shown in Fig. 5.3 was used to investigate the dynamics of onion skin cells [5.18]. Here an 8-bit CCD chip with 4.65m pixel pitch and 800×800 pixels exposed was used as the sensor. Only change with respect to the one for the

experiments mentioned in previous section was the addition of a lens in the reference arm to match the curvatures of the object and reference wavefronts. Photographs of the experimental setup are shown in Fig. 5.10.

For 3D imaging using interference microscopy, the object wavefront (transmitted through the cells) were made to interfere with a reference wavefront at the CCD. Photograph of the whole experimental setup as well as the close-up view of the interfering beams at the CCD is shown in Fig. 5.10a and 5.10b respectively.

The sample was placed on a glass cover slip. A condenser lens was used to increase the intensity of light falling on the portion of interest of the onion skin. A 10×, 0.25NA microscopic objective was used for magnification. To study the dynamics of onion skin cells, holograms were recorded regularly. Since the dynamics involved in these cells are slow, the recording interval was several hours.

Fig. 5.11 shows one of the recorded holograms. The image is not in focus because the image plane was situated behind the CCD plane (see Fig. 5.4). Since in digital holography, numerical focusing is possible, the scattered wavefront from the hologram plane is propagated to the image plane and the intensity and phase were computed.

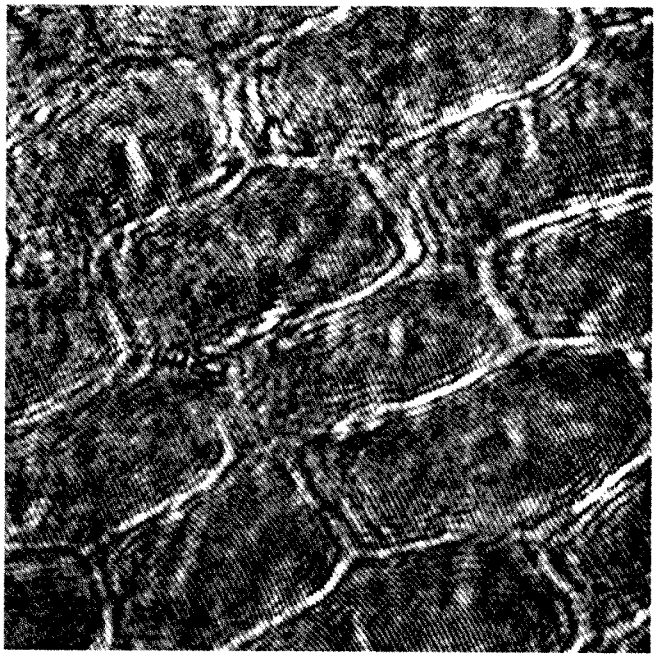

Fig. 5.11: Recorded hologram of onion skin section. Closely looking at the hologram, the micro- Interference fringes can be seen.

Fig. 5.12 shows the reconstructed intensity by propagating the angular spectrum due to the object component alone calculated by Fourier transforming the hologram multiplied by the reference wavefront and filtering out the other unwanted spatial frequencies. The Angular Spectrum Propagation integral given by Eq. (2.49) is used for the propagation. The image plane was situated 1cm behind the hologram plane. The phase of the object wavefront at the image plane is calculated by subtracting the phases obtained by numerical reconstruction of holograms recorded with and without the sample. This is shown in Fig. 5.13a. The 3D optical path length distribution is then computed using Eq. (5.2). This is shown in Fig. 5.13b.

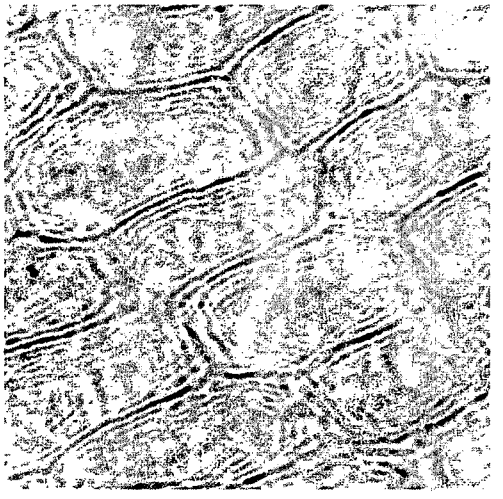

Fig. 5.12: Reconstructed intensity pattern at the image plane from the hologram shown in Fig.5.10.

From Fig. 5.13 it can be seen that the optical thickness distribution of onion skin cells are spherical in nature. Maximum thickness is at the centre and the thickness decreases as one move away from the centre. The average of the maximum thickness was 2.82μ. The same onion skin section was imaged two days. Fig. 5.14 shows the phase distribution as well as the optical path length distribution.

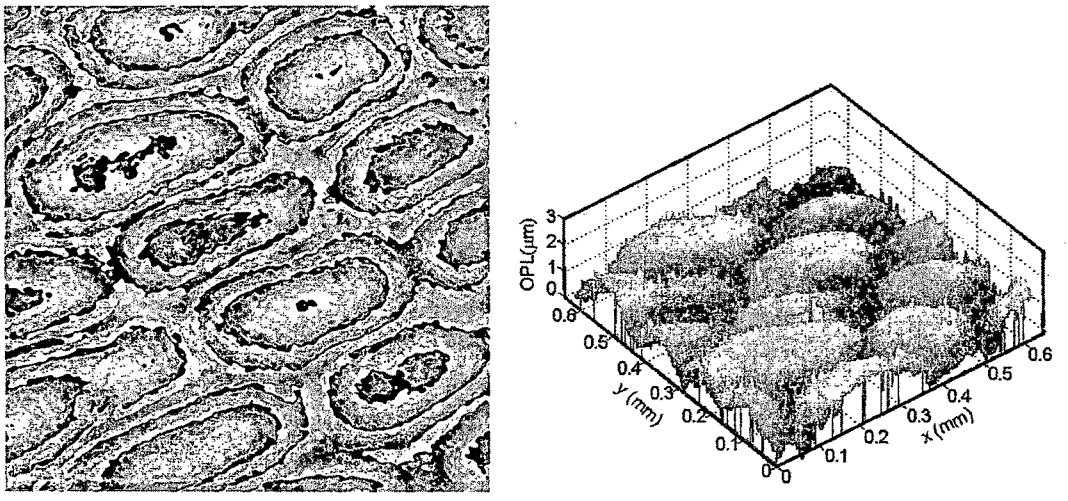

(a) (b)

Fig. 5.13: (a) Computed phase distribution for the onion skin cells (b) Calculated three dimensional optical path length distributions.

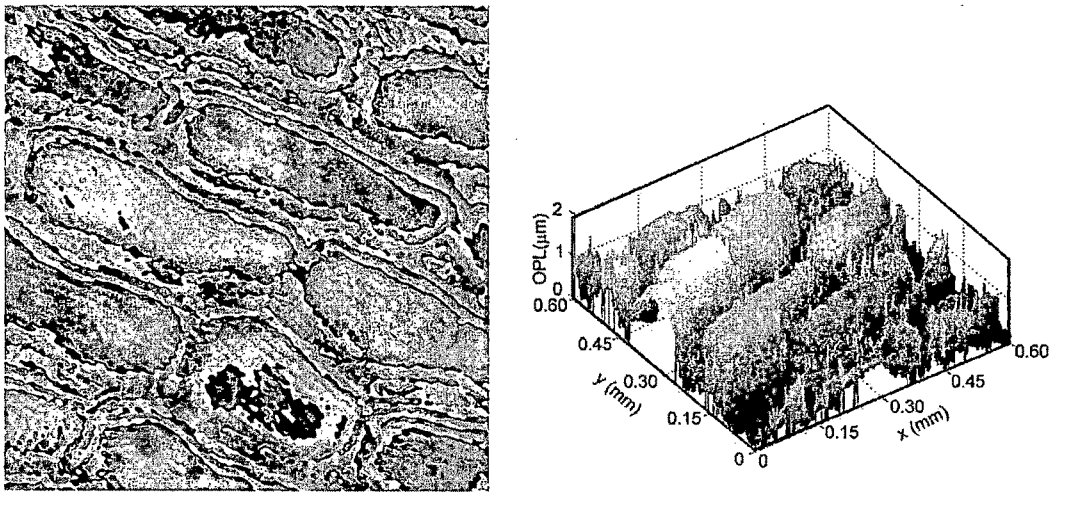

(a) (b)

Fig. 5.14: Phase difference after 48 hours. (a) Computed phase distribution (b) Calculated three dimensional optical path length distribution.

From Fig. 5.14 it can be seen that the optical path length has decreased compared to a fresh specimen. The average of the maximum optical path length change was 1.62μ in this case. The change might be due to the change in water content of the cells.

5.6.3 Experiments on Acrylic sheet

Letters embossed on a section of acrylic sheet was investigated secondly using digital holographic microscope [5.18]. Fig. 5.15 shows the recorded hologram for a section of the investigated object. A section of the object with a part of the embossed letter was imaged using a 20×, 0.4NA microscopic objective. From the hologram and the intensity reconstruction it is difficult to see even the edge of the object. This emphasizes the need of phase contrast imaging. Fig. 5.15c is the phase contrast image, which bring out the various aspects of the object.

The embossed PMMA slab was exposed to heat and acted as dynamic micro-object. The object was heated as shown in Fig. 5.16. The embossed portion was imaged using a 10×, 0.25NA microscopic objective on to the CCD, which then interferes with the reference beam to yield holograms. The image plane was 5mm after the hologram plane. An iron cylinder 6mm in diameter served as the heat source. It was heated up to 393K and was introduced suddenly below the object. Holograms were sampled at a frequency of 3Hz and stored in the PC. The heat source was removed after 70s and the sample was allowed to cool. A total of 361 holograms were recorded (120s) during the heating and cooling periods. The reconstructed phase at each time instance was subtracted from the phase distribution before heating started to yield the spatial as well as temporal change in optical path length.

Fig. 5.17 shows a series of phase maps for different time instances. The unwrapped phase maps were used to determine the change in optical path lengths. The figures show that the optical path length change increases as heating progress. The optical path length change is indicative optical and physical changes. The change may be due to change in refractive index (an optical property) of the medium under investigation or due to the change in the physical thickness of the medium. The phase information shown in Fig. 5.17 does contain noise levels, which sometimes make it impossible to perform phase unwrapping. The need for phase unwrapping can be eliminated either

by using a source with long wavelength or generating a synthetic wavelength by multi-wavelength recording [5.19-5.22].

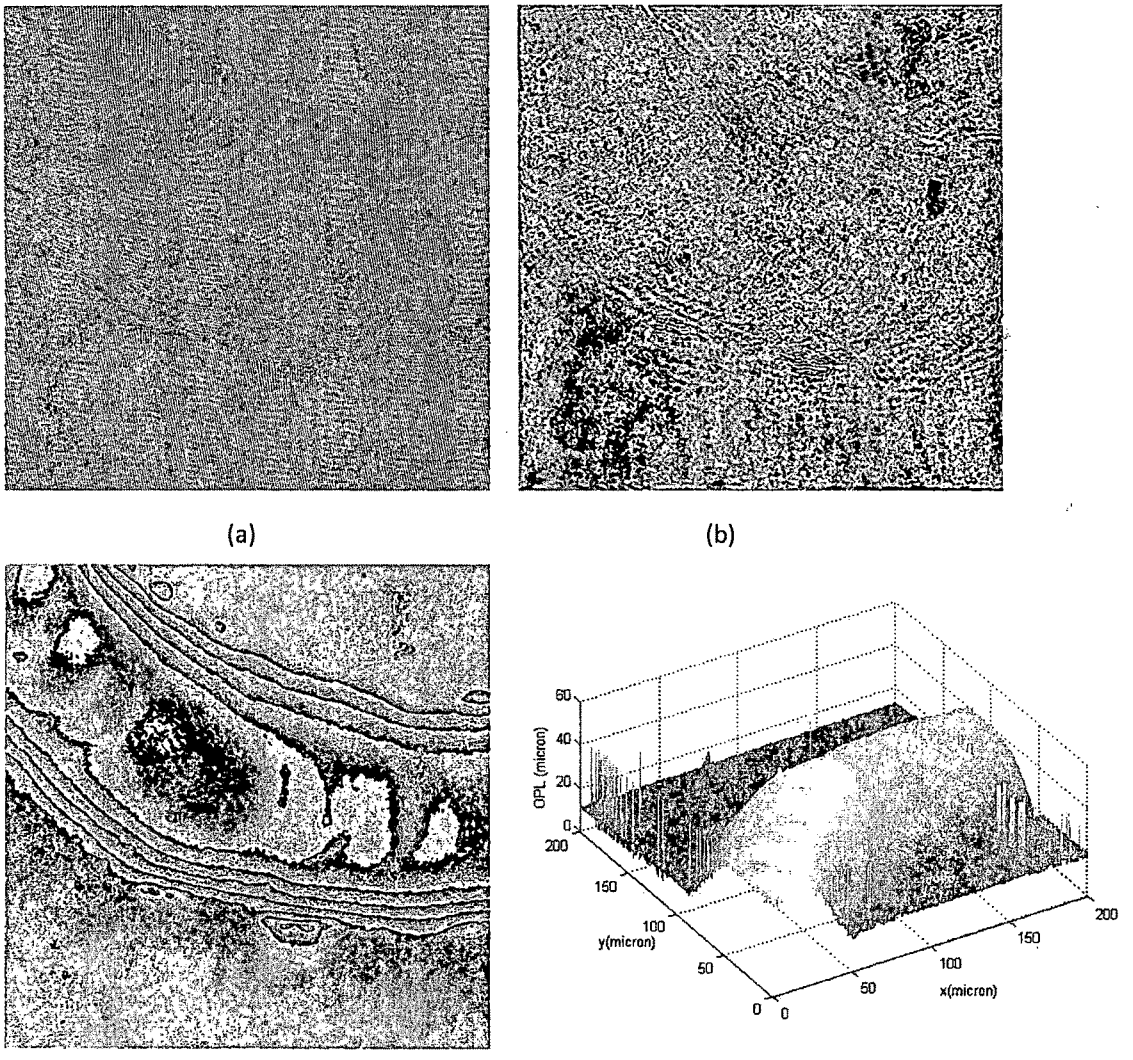

Fig. 5.15: (a) Hologram of the acrylic section with a portion of the embossed letter imaged with a 20X microscopic objective. (b) Reconstructed intensity at the image plane (c) Computed phase at the image plane (d) Optical path length distribution of the object.

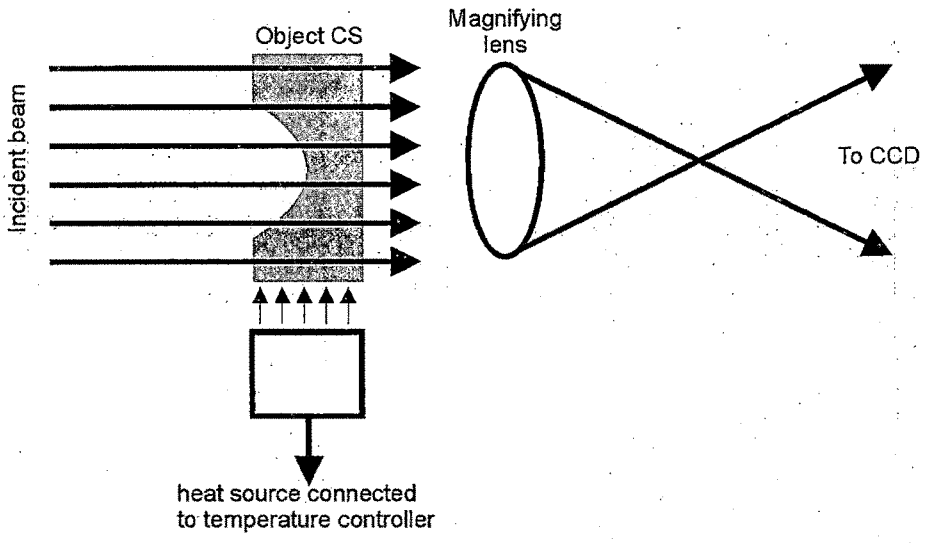

Fig. 5.16: Heating mechanism for studying the thermal dynamics of the acrylic slab using Digital interference holography

Fig. 5.18 shows the maximum optical path length change in the investigated medium as a function of time. The maximum path length change increases with time as the thermal diffusion process proceeds. After the heat source is removed the maximum optical path length change decreases with time but a lower rate, indicating cooling happens at a lower rate than heating.

The spatial variation of optical path length with time is shown in Fig. 5.19 for several time instances along the line shown in Fig. 5.17. The spatial change in optical path length can be used to obtain local refractive index changes by tomographic inversion of the chord integrated values. These refractive index values are used to compute the change in temperature by knowing the physical thickness and temperature coefficient of refractive index [5.23]. Measurement of change in temperature at a given spatial point with time, will lead to the determination of thermal conductivity as well as the thermal diffusion coefficient of the system under investigation.

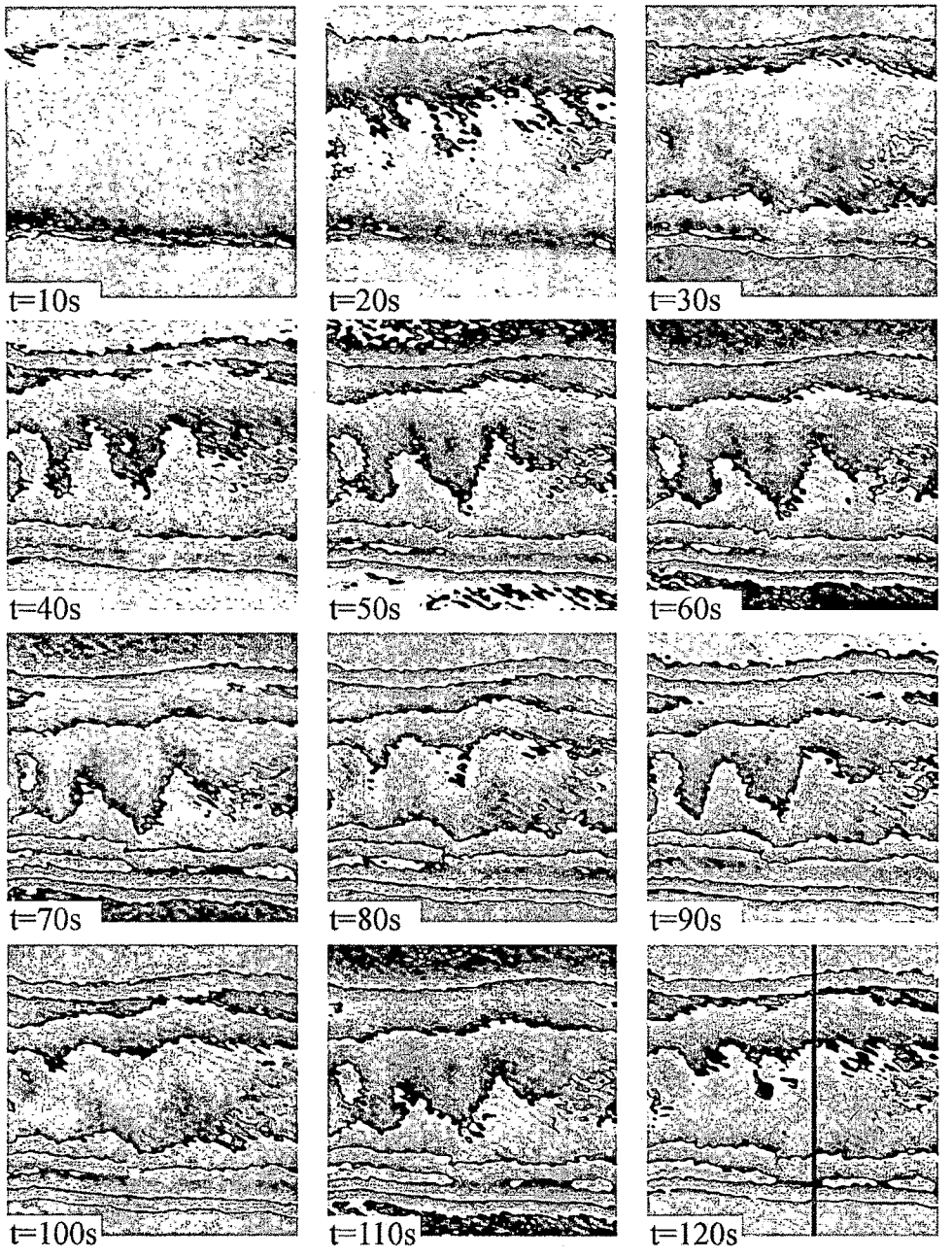

Fig. 5.17: Spatial and temporal variation in measured phase change with time. The heating source was removed after 70s. Heating was from top to bottom (magnifying lens forms an inverted image). The spatially varying optical path length change for several time instances along the line shown in the last figure is shown in Fig. 16.

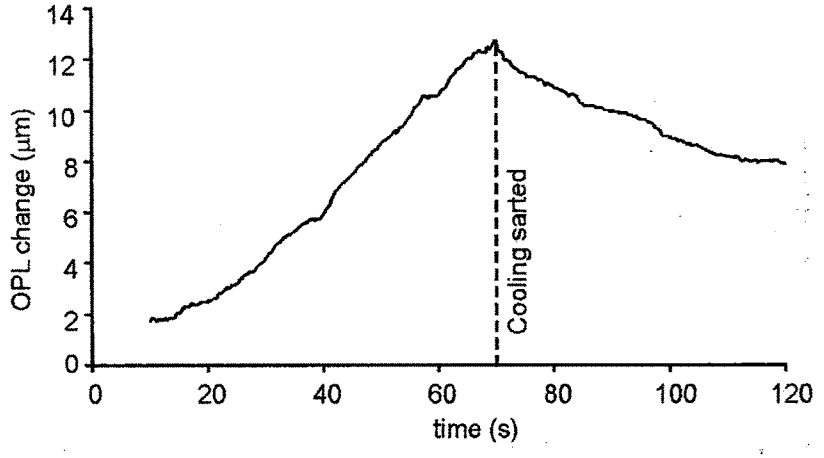

Fig. 5.18: Variation in maximum optical path length as a function of time. The heat source was suddenly removed after 70s. The plot indicate the different heating and cooling rate of the investigated system

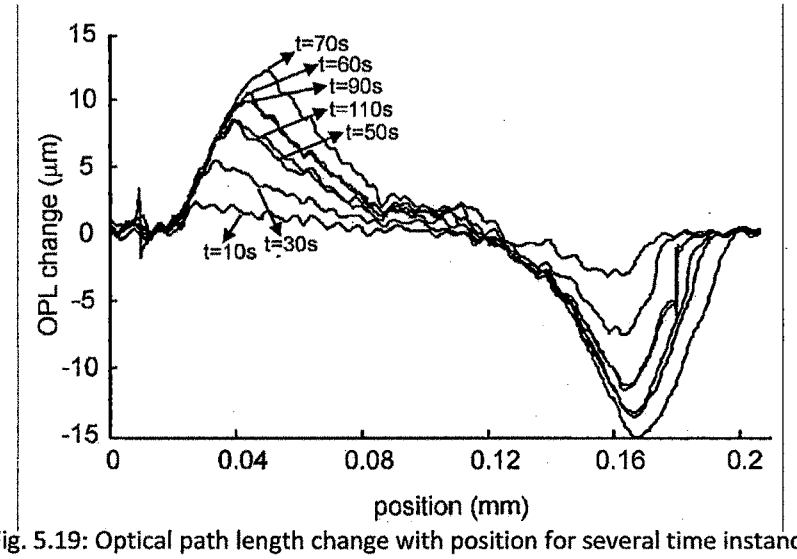

Fig. 5.19: Optical path length change with position for several time instances. The decrease in maximum optical path length change can be seen after the heat source was removed.

5.7 Discussions and conclusion

Digital holographic microscopy with angular spectrum propagation reconstruction was used for real-time quantitative phase contrast imaging of dynamic phase objects. The phase contrast images sheds information on the change of path length of the

probe beam propagating through the medium under investigation. This change in path length is due to either a change in refractive index or a change in thickness of the micro-object. The lateral as well as axial extent of the object can be determined using this method. It has been shown that DHM can be a useful tool for investigating dynamic phenomena occurring in such phase objects. To investigate the use of DHM to probe dynamic phenomena, an object when subjected to heat was studied. The reconstructed phase distribution can yield many important physical parameters of the object such as its thermal conductivity and thermal diffusion coefficient. The method can also be easily applied to micro-organisms for their detection, tracking as well as for studying their time evolution. Another aspect of the proposed method is that the dynamics of micro-organisms like bacteria under different temperature conditions can be imaged and quantified.

References

[5.1] MicrospcopyP - http://www.olympusmicro.com

[5.2] D. B. Murphy, *Fundamentals of light microscopy and electronic imaging*, Wiley-Liss, New York (2001).

[5.3] F. Zernike, "Phase contrast, a new method for microscopic observation of transparent objects", Physica, **9**, 686, (1942).

[5.4] F. Zernike, "Phase contrast, a new method for microscopic observation of transparent objects: PartII," Physica, **9**, 686, (1942).

[5.5] U. Schnars and W. Jueptner, Digital Holography: Digital hologram recording, numerical reconstruction and related techniques, Springer, Berlin (2005).

[5.6] U. Schnars and W. Jueptner, "Digital recording and numerical reconstruction of holograms," Meas. Sci. Technol., **13**, R85 (2002).

[5.7] E. Cuche, F. Bevilacqua and C. Depeursinge, "Digital holography for quantitative phase-contrast imaging," Opt. Lett., **24**, 291 (1999).

[5.8] P. Marquet, B. Rappaz, P. J. Magistretti, E. Cuche, Y. Emery, T. Colomb and C. Depeursinge, "Digital holographic microscopy: a noninvasive contrast imaging technique allowing quantitative visualization of living cells with subwavelength axial accuracy," Opt. Lett., **30**, 468, (2005).

[5.9] I. K. Moon, M. Daneshpanah, A. Stern, and B. Javidi, "Automated three-dimensional identification and tracking of micro/nano biological organisms by computational holographic microscopy," Proc. IEEE J., **97**, 990, (2009).

[5.10] C. J. Mann, L. Yu, C. Lo and M. K. Kim, "High-resolution quantitative phase-contrast microscopy by digital holography", Opt. Express, **13**, 8693 (2005).

[5.11] M. K. Kim, L. Yu and C. J. Mann, " Interference techniques in digital holography", J. Opt. A: Pure Appl. Opt., **8**, S518 (2006).

[5.12] E. Shaffer, N. Pavillon, J. Kuhn, C. Depeursinge, "Digital holographic microscopy investigation of second harmonic generated at a glass/air interface," Opt. Lett., **34**, 2450 (2009).

[5.13] Y. Frauel, T. Naughton, O. Matoba, E. Tahajuerce, and B. Javidi, "Three Dimensional Imaging and Display Using Computational Holographic Imaging", Proc. of the IEEE Journal, **94**, 636 (2006).

[5.15] P. Ferraro, S. Grilli, D. Alfieri, S. De Nicola, A. Finizio, G. Pierattini, B. Javidi, G. Coppola, and V. Striano, "Extended focused image in microscopy by digital Holography", Opt. Express, **13**, 6738 (2005).

[5.16] W. Osten and P. Ferraro, "Digital Holography and Its Application in MEMS/MOEMS Inspection," in Optical inspection of microsystems, W. Osten Ed. Taylor & Francis, (2007).

[5.17] F.Merola, L. Miccio, M. Paturzo, S. De Nicola and P. Ferraro: "Full characterization of the photorefractive bright soliton formation process using a digital holographic technique", Meas. Sci. Technol. **20**, 045301 (2009).

[5.18] L. Miccio, A. Finizio, S. Grilli, V. Vespini, M. Paturzo, S. De Nicola and P. Ferraro, "Tunable liquid microlens arrays in electrode-less configuration and their accurate characterization by interference microscopy", Opt. Express, **17**, 2487 (2009).

[5.19] A. Anand, V. V. Chhaniwal, B. Javidi, "Real-time Digital Holographic Microscopy for Phase Contrast 3D Imaging of Dynamic Phenomena", IEEE J. Disp. Technol., In press (2010).

[5.20] E. Allaria, S. Brugioni, S. De Nicola, P. Ferraro, S. Grilli and R. Meucci, "Digital holography at 10.6 μm", Opt. Commun. **215** 257 (2003).

[5.21] C. J. Mann, P. R. Bingham, V. C. Paquit, and K. W. Tobin, "Quantitative phase imaging by three-wavelength digital holography", Opt. Express, **16**, 9753 (2008).

[5.22] P. Ferraro, S. Grilli, L. Miccio, D. Alfieri, S. De Nicola, A. Finizio, and B. Javidi, Full color 3-D imaging by digital holography and removal of chromatic aberrations", IEEE J. Display Technol. **4**, 97(2008).

[5.23] P. Ferraro, L. Miccio , S. Grilli, M. Paturzo, S. De Nicola, A. Finizio, R. Osellame, and P. Laporta, "Quantitative Phase Microscopy of microstructures with extended measurement range and correction of chromatic aberrations by multiwavelength digital holography", Opt. Express, **15**, 14591 (2007).

[5.24] A. Anand, V. K. Chhaniwal, G. Pedrini, W. Osten, " Digital holographic tomography of phase objects", Proc. SPIE, **7389**, 73890L, (2009).